

MULTIGRID METHODS USING BLOCK FLOATING POINT ARITHMETIC

NILS KOHL*, STEPHEN F. MCCORMICK†, AND RASMUS TAMSTORF‡

Abstract. Block floating point (BFP) arithmetic is currently seeing a resurgence in interest because it requires less power, less chip area, and is less complicated to implement in hardware than standard floating point arithmetic. This paper explores the application of BFP to mixed- and progressive-precision multigrid methods, enabling the solution of linear elliptic partial differential equations (PDEs) in energy- and hardware-efficient *integer arithmetic*. While most existing applications of BFP arithmetic tend to use small block sizes, the block size here is chosen to be maximal such that matrices and vectors share a *single* exponent for all entries. This is sometimes also referred to as a scaled fixed-point format. We provide algorithms for BLAS-like routines for BFP arithmetic that ensure exact vector-vector and matrix-vector computations up to a specified precision. Using these algorithms, we study the asymptotic precision requirements to achieve discretization-error-accuracy. We demonstrate that some computations can be performed using as little as 4-bit integers, while the number of bits required to attain a certain target accuracy is similar to that of standard floating point arithmetic. Finally, we present a heuristic for full multigrid in BFP arithmetic based on saturation and truncation that still achieves discretization-error-accuracy without the need for expensive normalization steps of intermediate results.

Key words. Block floating point, fixed point, mixed precision, multigrid

AMS subject classifications. 65F10, 65G50, 65M55

1. Introduction. Floating point arithmetic is used to perform almost all scientific computations. At the same time, it is well known that integer arithmetic, where applicable, is less complicated to implement in hardware than standard floating point arithmetic [16] and it is generally more energy efficient. As an example, the actual arithmetic associated with 32 bit integer based addition requires roughly an order of magnitude less energy than the corresponding floating point operation, [8, 9]. For this reason, *fixed point* formats are typically preferred in embedded computing where resources are limited. Unfortunately, the inherent range limitation of fixed point formats renders them difficult to use for the numerical approximation of partial differential equations (PDEs). A compromise is to use a BFP format: a block of fixed point mantissas along with a *shared exponent* [20]. In this way, the range of representable numbers in BFP formats can be adapted dynamically, while all computations are still performed in pure integer arithmetic. While the notion of BFP and fixed point formats goes back quite far in the history of computing, it has recently gained renewed popularity for neural network training, e.g., [10, 5, 12, 18, 4, 17, 14, 15, 2]. The actual cost of arithmetic is typically dwarfed by the cost of memory access, but [14] shows that it is possible to increase the overall energy efficiency by an order of magnitude when using BFP compared to using the mixed FP16/FP32 arithmetic in Nvidia’s tensor cores.

In this paper, we study the solution of linear systems arising from the discretization of elliptic PDEs in BFP arithmetic using mixed- and progressive-precision multigrid methods. As in [13, 19], we are interested in the asymptotically optimal choice of precisions that guarantees discretization-error-accurate solutions. We design algorithms for matrix-vector and vector-vector operations in BFP-arithmetic that ensure

*Friedrich-Alexander-Universität Erlangen-Nürnberg, Germany (nils.kohl@fau.de).

†University of Colorado at Boulder, Boulder, CO (stephen.mccormick@colorado.edu).

‡Walt Disney Animation Studios, Burbank, CA (rt@acm.org).

efficient and exact computations up to a specified target precision, and emphasize that all computations are performed in two’s complement integer arithmetic.

To ensure exact computations, we leverage the fact that BFP enables the computation of the exact inner product between two vectors at a reasonable cost [5]. The exact dot product can also be computed for standard floating point numbers using the method proposed by Kulisch [11], and this method is used by posits to implement the so-called “quire”, [6]. However, in general it requires a very large accumulator with more than 4,000 bits for double precision floating point numbers and more than 65,000 bits for quad-precision numbers. For block floating point numbers, the bulk of the computation can be done in fixed point arithmetic where all the elements are stored in the same format. The size of the accumulator for the result of the exact BFP dot product therefore only grows logarithmically with the number of vector entries. Thus, the technique in [3] can be used to compute an exact dot product for high-precision inputs using on the order of 100 – 200 bits or less for most practical cases.

The outline of the remaining parts of the paper is as follows: Section 2 introduces the BFP-format and its most relevant properties. Section 3 analyses the relative energy error induced by BFP-quantization. Section 4 develops BFP-specific algorithms for mixed-precision matrix-vector and vector-vector operations. Section 5 summarizes the results of [13, 19] and extends the mixed-precision multigrid method defined therein to BFP-arithmetic. Section 6 provides a numerical study of the precision requirements for the BFP-multigrid solver in order to achieve discretization-error-accurate approximations in the energy norm for two model problems. We end in Section 7 with concluding remarks.

2. Block floating point arithmetic. We define BFP numbers by a block of integers (also referred to as mantissas) equipped with a shared factor that is an integer power of two. All integers of a block have the same bit-width, and we assume standard two’s complement representation. We denote the set of two’s complement integers with bit-width $w \in \mathbb{Z}_{>0}$ as $\mathbb{X}_w := [-2^{w-1}, 2^{w-1} - 1] \cap \mathbb{Z}$. The block will typically be a vector or matrix, but the concept generalizes to any type of tensor or irregular structures such as sparse matrix formats. We denote the set of BFP numbers by \mathbb{B} and write each element as a tuple

$$(2.1) \quad (x_e, x_m, x_w, x_d) \in \mathbb{B}.$$

In this notation, $x_e \in \mathbb{Z}$ denotes the shared exponent, and $x_w \in \mathbb{Z}_{>0}$ denotes the fixed bit-width of the mantissas. With a slight abuse of notation, we let $x_m \in \mathbb{X}_{x_w}^{x_d}$ denote the block of mantissas, where x_d represents the layout of the elements in the block. In the case of an n -dimensional vector, we let $x_d = n$, and in the case of an $n \times n$ matrix, we write $x_d = n \times n$. We allow the exponent x_e to be chosen arbitrarily because it is shared over the entire block and its storage cost is negligible in practice. (A 64-bit integer exponent is likely more than sufficient for most practical use cases.) We use the notation $x \sim (x_e, x_m, x_w, x_d)$ to denote that x is the block of rational numbers $x = 2^{x_e} \cdot x_m$, and the shorthand $\mathbb{B}^d = \{(x_e, x_m, x_w, x_d) \in \mathbb{B} : x_d = d\}$.

Generally, multiple equivalent representations of x correspond to different choices of x_e . We call the representation (x_e, x_m, x_w, x_d) of $x \neq \mathbf{0}$ *normalized* if x_e is minimal (possibly negative). In the following, $x \in \mathbb{B}$ is used to refer to both the tuple containing the representation for the BFP numbers and the represented numbers.

Relevant properties of a BFP format can be derived from the quantities x_e and x_w . As an example, the range of all entries of x is $[-2^{x_w-1} \cdot 2^{x_e}, (2^{x_w-1} - 1) \cdot 2^{x_e}]$,

and all the representable numbers are equidistantly separated with distance 2^{x_e} . The precision of a normalized BFP tensor with a fixed mantissa width x_w therefore depends on the value of the entry that has the largest magnitude. To relate floating point precision (i.e., unit roundoff) to the BFP context, we refer in this paper to the precision of a BFP format as $\varepsilon = 2^{-(x_w-1)}$. This is the spacing between two adjacent values in a normalized BFP tensor with entries in the range $[-1, 1 - \varepsilon]$.

We use standard two's complement integer arithmetic for addition, subtraction, and multiplication, as well as arithmetic left- (\ll) and right-shifts (\gg). Additionally, we define the operation $\text{decr}(b, \cdot)$ that truncates the $b \geq 0$ leftmost bits of a two's complement integer (corresponding to casting to a narrower integer type), and the operation $\text{incr}(b, \cdot)$ that prepends b bits that all have the value of the most significant bit (MSB) to the left (corresponding to casting to a wider type). Truncation of the rightmost bits is realized via arithmetic right-shifts, which implies rounding towards negative infinity for signed two's complement integers.

REMARK 1 (Block size). *Throughout this paper, we consider the extreme case that each vector or matrix is represented by a single block. At the other extreme, setting the block size x_d to 1 is equivalent to using standard floating point arithmetic. From an implementation standpoint, these extreme cases (block sizes 1 and maximal) are special, as block-boundaries can be ignored. However, there may be practical reasons to split up a vector or matrix into multiple blocks. As an example, hardware components may be specialized to perform optimized arithmetic on relatively small block sizes (e.g., on the order 10 – 100 entries) [18, 4]. That being said, choosing the block size maximally has to be the worst case in terms of quantization. Thus, the results presented herein are expected to extend easily to smaller block sizes.*

REMARK 2 (BFP dot products). *The energy saving potential of BFP arithmetic compared to standard floating point arithmetic is rooted in the simplification of the dot product. This carries over to matrix-vector and matrix-matrix multiplications, which conceptually are just consecutive dot products. When solving sparse linear systems using iterative solvers, the critical steps to performance are sparse matrix-vector multiplications, which makes an efficient dot product particularly beneficial.*

To understand the origin of the complexity reduction, consider the addition of two floating point numbers. Before the mantissas can be added, they have to be aligned by right-shifting one of them in order to ensure that the exponents are equal. After the addition, the result has to be normalized, which requires another shift operation. This is somewhat simplified, but illustrates the complexity of a seemingly simple operation. A dot product of two vectors $a, b \in \mathbb{R}^n$ with at most m_A non-zero elements per vector requires $m_A - 1$ additions and, therefore, if performed in floating point arithmetic, $2(m_A - 1)$ arithmetic shifts. This is different in BFP arithmetic: assuming that the block sizes are maximal, the alignment step is not necessary at all, since the terms in the sum in the dot product all share the same exponent. (This exponent is computed by adding the block-exponents of a and b .) Furthermore, normalization is only necessary after summing up the result in a sufficiently large register. In other words, only a single arithmetic shift is necessary in BFP arithmetic compared to $2(m_A - 1)$ arithmetic shifts in floating point arithmetic.

A key assumption here is that the accumulator is sufficiently large to hold the sum without overflow. Since the number of non-zero terms in the sum is assumed to be at most m_A , it follows that the size of the accumulator grows with $\log_2(m_A)$. In practice, m_A is typically at most in the hundreds, so only a relatively few additional bits are required to compute the exact dot product. With suitable rounding, this number could

possibly be reduced.

3. Relative BFP-quantization error. A critical issue concerning the practical use of BFP arithmetic is its effect on accuracy. The empirical observations in [13, 19] suggest that the relative fixed-point quantization error is $\mathcal{O}(\kappa^{\frac{1}{2}}\varepsilon)$, and our experience indicates that BFP exhibits the same order. The aim in this section is to develop theoretical results that shed more light on this issue. In particular, we provide an abstract bound that suggests that BFP quantization might incur a slightly higher order of error. We then argue that this bound might be pessimistic in that it does not fully take finite-precision into account.

To be specific, let A denote the symmetric positive definite (SPD) system matrix of an elliptic PDE discretized by standard finite elements on a uniform $n \times n$ grid in the unit square. Assume for simplicity that A is scaled so that its minimal eigenvalue is $\mathcal{O}(1)$. With u an infinite-precision vector in \mathbb{R}^{n^2} having unit infinity norm $\|u\|_\infty$, write $u = v + \varepsilon z$, where v results from BFP quantization in ε precision and εz is the quantization error. Note that $\|u\|_\infty = \|v\|_\infty = 1$ and $\|z\|_\infty \leq 1$, where $\|\cdot\|_\infty$ denotes the infinity norm. The goal is then to bound the relative BFP quantization error $\mathcal{E}(v, z) := \frac{\varepsilon\|z\|_A}{\|v\|_A}$, where $\|\cdot\|_A = \|A^{\frac{1}{2}} \cdot\|$ denotes the energy norm written in terms of the Euclidean norm $\|\cdot\|$.

We can usually choose z so that it has maximum order, that is,

$$(3.1) \quad \|z\|_A = \mathcal{O}(\kappa^{\frac{1}{2}}n),$$

while preserving the property that the BFP quantization of u is v . For example, with the five-point discrete 2D Poisson equation, we could choose z to alternate between 1 and 0 in a checkerboard fashion. This choice means that BFP truncation of u does indeed result in v (as might not be the case with negative values of v) and it also assures that (3.1) holds: z is oscillatory in that $\|z\|_A = \mathcal{O}(\kappa^{\frac{1}{2}})\|z\|$ and it possesses enough 1's to make $\|z\| = \mathcal{O}(n)$. To bound $\mathcal{E}(v, z)$ in this case, we therefore need only find a lower bound for $\|v\|_A$.

We have not been able to establish a sharp lower bound for $\|v\|_A$ theoretically because it ostensibly requires the discrete optimization of $\|v\|_A$ over the space of vectors of unit infinity norm that are represented exactly in ε precision. We can, however, obtain a potentially loose lower bound by ignoring the finite-precision restriction and exploiting the fact that the minimum value of $\|v\|_A$ is the inverse of the square root of the maximum of the diagonal entries of A^{-1} . (See Appendix A.) Our numerical estimates of A^{-1} for the model 2D Poisson problem for $n \in \{1, 2, \dots, 100\}$ indicate that the minimum value of $\|v\|_A$ is bounded below by a constant times $n^{0.994}$, suggesting that $\mathcal{E}(v, z)$ might grow slightly faster than $\mathcal{O}(\kappa^{\frac{1}{2}}\varepsilon)$ (by a factor of $n^{0.006}$).

The slightly larger bound requires u to be very smooth while the part εz that is truncated away is oscillatory. While we do not know how likely this is, we have not experienced an error growth that is larger than $\mathcal{O}(\kappa^{\frac{1}{2}}\varepsilon)$. Just for illustration, Figure 1 shows $\kappa^{\frac{1}{2}}\varepsilon$ and the relative energy error after quantization to BFP over refinement for different mantissa widths v_w . The precision ε is computed as described in Section 2. We chose v as the quantized eight eigenvectors v_i of A that belong to the eight smallest eigenvalues λ_i , $i = 1, \dots, 8$, since those yielded the largest relative errors. (Note that the errors are getting smaller as i increases.) The model problems are discussed in Section 6.

In any case, a possible reason for the discrepancy between theory and our experience is that the theory is only an upper bound. Indeed, since v has not been

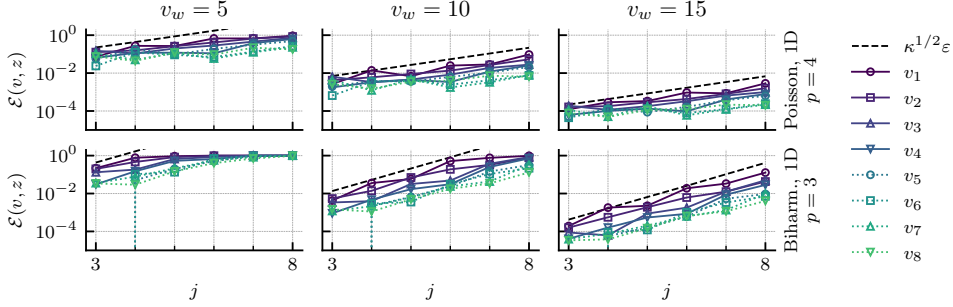


FIG. 1. Relative energy errors $\mathcal{E}(v, z) := \varepsilon \|z\|_A / \|v\|_A$ after quantization of 8 eigenvectors u_i of A for the model problem discussed in Section 6. The precision is indicated by the mantissa width $v_w \in \{5, 10, 15\}$. The x-axis shows the refinement level, j , with corresponding mesh sizes $h = 2^{-j}$.

restricted to ε -precision in this theoretical bound, it may be an overestimate due to the theoretical minimum being taken over a wider set.

4. BLAS operations using BFP. The majority of iterative solvers for linear systems of equations is composed of vector-vector and matrix-vector operations. In our case, most computations can be written in the form

$$(4.1) \quad z \leftarrow \alpha Ax + \beta y,$$

with $y, z \in \mathbb{R}^n$, $x \in \mathbb{R}^m$, $A \in \mathbb{R}^{n \times m}$, $\alpha, \beta \in \mathbb{R}$. This operation is also known as the generalized matrix-vector multiplication (**gemv**) from the Basic Linear Algebra Subprograms (BLAS) specification [1]. It can be simplified in some cases, such as when $A = I$ (**axpby**), $y = \mathbf{0}$, or $\alpha = 1$.

One contribution of this paper is the realization of a framework for such vector operations that is suited for mixed-precision computations using BFP arithmetic with a focus on the requirements for multigrid methods. We assume that all inputs are given in a normalized BFP format with arbitrary, and possibly different, mantissa widths and block-exponents. The desired width of the mantissa of the result, denoted w_{out} , is assumed to be specified as an input parameter, and the result is required to be normalized and computed *exactly* up to chosen size of the mantissa.

The normalization of the result is not straightforward, since we generally do not know the largest MSB index of the block-mantissa before the entire vector has been computed. Two naive implementations come to mind:

- (a) (*computationally efficient*) The entire result is computed exactly and *stored* in a temporary unnormalized BFP vector using a sufficiently wide mantissa. The MSB index is tracked. In a second step, the block-mantissa is shifted to normalize the result, and then quantized to w_{out} .
- (b) (*memory efficient*) The result is first computed exactly element by element only to track the MSB index for the entire block. The actual result is discarded after the computation of each element. In a second step, the result is *recomputed* element by element with each element being shifted to ensure that the overall block is normalized. The result is also quantized to w_{out} bits.

Both approaches have disadvantages. In (a), the entire temporary BFP vector carrying the exact result must be allocated. Depending on the precision and block-exponents of the input variables, the amount of memory required can be huge. In (b), the exact result is not stored at all. Only the quantized result is stored, but

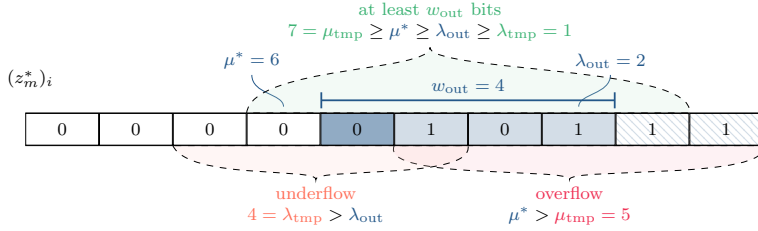


FIG. 2. Illustration of the bit indices in Algorithm 1. The bit string $(z_m^*)_i$ shown here represents one element of the block-mantissa z_m^* of the exact result $z^* \in \mathbb{B}^n$. We assume for simplicity that this element has the maximum MSB index of all elements in z_m^* . The actual MSB and LSB indices of the relevant portion (filled boxes) of $(z_m^*)_i$ are μ^* and λ_{out} . We show three example bit-‘windows’ that are sufficient (top), or result in underflow (bottom left), or overflow (bottom right). Only if the estimated MSB and LSB indices μ_{tmp} and λ_{tmp} (example choices are displayed in the figure) that are derived from γ and w_{tmp} fulfill $\mu_{tmp} \geq \mu^* \geq \lambda_{out} \geq \lambda_{tmp}$, are all relevant bits (filled boxes) captured by the window. Otherwise, we either obtain underflow or overflow (illustrated by example choices for λ_{tmp} and μ_{tmp}).

this roughly doubles the computational effort. We suggest a compromise of these two approaches, where the temporary result is neither stored exactly nor discarded but rather quantized to some intermediate width $w_{tmp} \geq w_{out}$. The idea is to choose the width large enough so that at least w_{out} ‘good’ bits are left for the largest element after normalization of the entire block, but still small enough so that much less memory is allocated than would be required for the exact result.

This algorithm requires a (preferably sharp) upper bound $\gamma \geq \|z\|_\infty$ and a number of bits w_{tmp} to prescribe a ‘window’ in the mantissa of the exact result that ideally contains the most significant w_{out} bits. When the result is computed, only those w_{tmp} bits that make up that window are stored. Everything beyond the window is discarded.

In the following, indices are used to refer to individual bits of a bit string. The rightmost bit is assigned index 0, with incrementing indices to the left. To refer to a substring of a bit string, we use μ (mu) to refer to the index left to the MSB (leftmost bit) of that substring, and λ (lambda) to refer to the index of its least significant bit (LSB) (rightmost bit). For convenience, μ is set to the bit-index to the left of the actual MSB of the substring, so that the width of the substring is $\mu - \lambda$. For example, given a bit string 00010010, its substring 1001 is indicated by $\mu = 5$, and $\lambda = 1$. Its width is $\mu - \lambda = 4$.

After looping through the entire result vector, we know the MSB index μ^* of the exact mantissa (we denote variables corresponding to exact quantities using asterisks). Therefore, we can determine whether at least w_{out} ‘good’ bits have been collected. If that is the case, the temporary result is shifted and quantized to w_{out} bits. We slightly abuse the terms overflow and underflow to refer to the cases where we either do not capture the MSB or capture less than w_{out} relevant bits of the mantissa entry with the maximum MSB index. In such cases, the result has to be recomputed. The mechanism is illustrated in Figure 2.

To implement the above procedure, we present an ‘outer’ algorithm `qcomp` in Algorithm 1 that ensures exact computation up to the specified precision w_{out} . The actual exact computation is specified by a pair of callback functions that are passed to `qcomp`. One of those functions sets up the precision and exponent, and the other performs the exact integer arithmetic for one element of the result vector. We need

Algorithm 1 Quantized BFP vector computation: `qcomp`

Input: `setup-func`, `comp-func`, `input`, $w_{\text{out}}, w_{\text{tmp}} : \mathbb{Z}_{>0}$, $\gamma : \mathbb{B}^1$, $n : \mathbb{Z}_{>0}$
Precondition: $0 < w_{\text{out}} \leq w_{\text{tmp}}$, $\gamma > 0$, γ normalized
Local variables: `setup`, $z^* : \mathbb{B}^1$ (exact result), $z_{\text{tmp}} : \mathbb{B}^n$ (temporary result),
 $z_{\text{out}} : \mathbb{B}^n$ (normalized result), $\mu_{\text{tmp}}, \lambda_{\text{tmp}}, \mu^*, \lambda_{\text{out}} : \mathbb{Z}$, `overflow`, `underflow` : `bool`

▷▷ **Allocation and setup.**

- 1: $(z^*, \text{setup}) \leftarrow \text{setup-func}(\text{input})$ ▷ Setup necessary variables for exact computations.
- 2: $\mu_{\text{tmp}} \leftarrow \text{msb}(\gamma_m) + \gamma_e - z_e^*$ ▷ MSB of the estimated mantissa window.
- 3: $\lambda_{\text{tmp}} \leftarrow \mu_{\text{tmp}} - w_{\text{tmp}}$ ▷ LSB of the estimated mantissa window.
- 4: $(z_{\text{out}})_w \leftarrow w_{\text{out}}$ ▷ Width of result BFP vector.
- 5: $(z_{\text{tmp}})_w \leftarrow w_{\text{tmp}}$ ▷ Width of temporary BFP vector.
- 6: $(z_{\text{tmp}})_e \leftarrow z_e^* + \lambda_{\text{tmp}}$ ▷ Block-exponent of truncated temporary result z_{tmp} .

▷▷ **Computation of temporary BFP vector.**

- 7: $\mu^* \leftarrow 1$ ▷ Keep track of the largest MSB idx. of the exact result.
- 8: **parallel for** $i = 1, \dots, n$ **do**
- 9: $z^* \leftarrow \text{comp-func}(z^*, \text{input}, \text{setup}, i)$ ▷ Compute exact quantity in parallel.
- 10: $\mu^* \leftarrow \text{atomic-max}(\mu^*, \text{msb}(z_m^*))$ ▷ Atomic update of the global max.
- 11: $z_m^* \leftarrow z_m^* \gg \lambda_{\text{tmp}}$ ▷ Shift and truncate exact result.
- 12: $((z_{\text{tmp}})_m)_i \leftarrow \text{decr}(z_w^* - (z_{\text{tmp}})_w, z_m^*)$ ▷ Cast result into temporary BFP vector.

13: **end parallel for**

▷▷ **Ensuring exact result up to w_{out} bits.**

- 14: $\lambda_{\text{out}} \leftarrow \mu^* - w_{\text{out}}$ ▷ LSB of the target mantissa window.
- 15: $(z_{\text{out}})_e \leftarrow z_e^* + \lambda_{\text{out}}$ ▷ Block-exponent of result z_{out} .
- 16: `overflow` $\leftarrow \mu_{\text{tmp}} < \mu^*$ ▷ Max. MSB index of exact result left of est. window.
- 17: `underflow` $\leftarrow \lambda_{\text{out}} < \lambda_{\text{tmp}}$ ▷ Captured less than w_{out} relevant bits.

18: **if** `overflow` \vee `underflow` **then**

▷▷ **Overflow or less than w_{out} meaningful bits. Recompute.**

- 19: **parallel for** $i = 1, \dots, n$ **do**
- 20: $z^* \leftarrow \text{comp-func}(z^*, \text{input}, \text{setup}, i)$ ▷ Recompute exact quantity in parallel.
- 21: $((z_{\text{out}})_m)_i \leftarrow \text{decr}(z_w^* - (z_{\text{out}})_w, z_m^* \gg \lambda_{\text{out}})$ ▷ Shift and truncate exact result.

22: **end parallel for**

23: **else**

▷▷ **At least w_{out} meaningful bits**

- 24: **parallel for** $i = 1, \dots, n$ **do**
- 25: $((z_{\text{out}})_m)_i \leftarrow \text{decr}(w_{\text{tmp}} - w_{\text{out}}, ((z_{\text{tmp}})_m)_i \gg (\lambda_{\text{out}} - \lambda_{\text{tmp}}))$ ▷ Truncate all bits that exceed the target window.

26: **end parallel for**

27: **end if**

28: **return** z_{out}

BFP-versions of the standard BLAS routines `axpy` ($z \leftarrow \alpha x + \beta y$) and `gemv` ($z \leftarrow \alpha Ax + \beta y$). For efficiency and simplicity, we use custom routines for the special cases $z \leftarrow x - y$ (`sub`) and $z \leftarrow Ax$ (`spmv`). The callbacks used for the exact matrix-vector multiplication `spmv` and the corresponding algorithms for `axpy` and `gemv` are listed in [Appendix B](#). We denote that a routine is wrapped by `qcomp` by prefixing it with `q`; for instance, we have `qspmv(...)` = `qcomp(espmv-setup, espmv-row, ...)`.

5. Mixed- and progressive-precision multigrid. As in [19], our goal is to approximate the solution of linear elliptic PDEs up to discretization-error-accuracy using arithmetic of minimal precision. Thus, we consider linear systems of the form

$Ax = b$ with $A \in \mathbb{R}^{n \times n}$ SPD, $x, b \in \mathbb{R}^n$. A balance of quantization, discretization, and algebraic errors must be obtained by an appropriate choice of the precisions employed during computation. The system is solved by iterative refinement (\mathcal{IR}) with an inner V-cycle (\mathcal{V}), possibly as part of full multigrid (\mathcal{FMG}). We apply subscripts to relate a quantity to a refinement level (for example, A_j refers to the discrete operator on level j). As in [19], three precisions $\check{\varepsilon}_j \leq \varepsilon_j \leq \dot{\varepsilon}_j$ are defined on each refinement level $j > 0$. The “working” precision, i.e., the precision of the computed result, is ε . It is used in \mathcal{IR} and \mathcal{FMG} , while the precision of the inner solver is reduced to $\dot{\varepsilon}$. To account for quantization errors induced by storing the input in finite precision, A and b are stored in $\check{\varepsilon}$ precision. A fourth, high precision $\bar{\varepsilon}_j \leq \varepsilon_j$ is required in [19] to ensure more precise computation of the residual in \mathcal{IR} . However, thanks to [Algorithm 1](#), we can assert that each result is computed exactly up to a specified precision, thereby allowing us to eliminate the need for $\bar{\varepsilon}_j$. Under certain assumptions, [19] shows that the precisions required to attain discretization-error-accuracy can be bounded by functions of the following quantities: the finite element polynomial of order k , the order $2m$ of the PDE, and the pseudo mesh size $h_j = \kappa_j^{-\frac{1}{2m}}$, where $\kappa_j := \| |A_j| \| \cdot \| A_j^{-1} \|$ ($|\cdot|$ denotes matrix entries replaced by their absolutes). In particular, it is shown that

$$(5.1) \quad \check{\varepsilon}_j \in \mathcal{O}(h_j^{k+m}), \quad \varepsilon_j \in \mathcal{O}(h_j^k), \quad \dot{\varepsilon}_j \in \mathcal{O}(h_j^m).$$

Following [Section 2](#) for the relation of floating point to BFP precision, we are now interested in the behavior of the total error with respect to the corresponding BFP mantissa widths \check{w}_j , w_j , and \dot{w}_j . Assuming that $2h_{j+1} = h_j$ and that [\(5.1\)](#) also applies to BFP arithmetic, then [\(5.1\)](#) suggests that the widths of the corresponding mantissas are related to refinement by

$$(5.2) \quad \check{w}_j \in \mathcal{O}((k+m)j), \quad w_j \in \mathcal{O}(kj), \quad \dot{w}_j \in \mathcal{O}(mj).$$

As an example, consider the solution of a second-order PDE ($m = 1$). According to [\(5.2\)](#), only 1 bit needs to be added per refinement level to the mantissa width \dot{w}_j used in the inner solver to ensure discretization-error-accuracy.

[Algorithms 12 to 14](#) list the BFP-versions of \mathcal{IR} , \mathcal{V} , and \mathcal{FMG} as defined in [19]. We refer to \mathcal{IR} with \mathcal{V} as the inner solver by $\mathcal{IR}\text{-}\mathcal{V}$. The BFP-routines require the width of the mantissa for the result w_{out} , an estimate for the infinity norm of the result γ , and the number of bits $w_{\text{tmp}} \geq w_{\text{out}}$ to be used for the mantissa of the temporary result. Note that line 7 in [Algorithm 12](#) (correction step) and line 6 in [Algorithm 14](#) (\mathcal{FMG} -prolongation) are the only calls where we use standard working precision $w_{\text{out}} = w$. For all remaining calls, we use low precision $w_{\text{out}} = \dot{w}$. We comment on the choice of γ and w_{tmp} in [Subsections 6.3](#) and [6.4](#) but omit them as input arguments to the BFP-routines in [Algorithms 12 to 14](#) for better readability.

Inside of \mathcal{V} ([Algorithm 13](#)) we use a second-order Chebyshev iteration for relaxation. We base our implementation on a simplification of [7, Algorithm 1]. When reduced to just two iterations and a zero initial guess, it can be implemented using a single call to `qgemv` as shown in line 2 of [Algorithm 13](#). This call requires two coefficients c_1, c_2 , which are estimated on refinement level $\ell_{\text{est}} = 5$, using [Algorithm 10](#). As in [19], the spectral radius $\rho(D^{-1}A)$ is estimated via the solution of the generalized eigenvalue problem $A_{\ell_{\text{est}}}x = \lambda D_{\ell_{\text{est}}}x$, and the targeted percentage of the spectrum η is determined empirically, by minimization of the V-cycle convergence rate over a set of values $\mu_i^* = i/100$, $i = 0, 1, \dots, 100$. After the computation of c_1 and c_2 , the simplification also requires a setup phase where we set $A_j \leftarrow D_j^{-1}A_j$, $b_j \leftarrow D_j^{-1}b_j$, and $R_j \leftarrow D_{j-i}^{-1}P^T D_j$ in order to avoid division operations (which are delicate in

BFP-arithmetic) during the relaxation step. See [Algorithm 11](#). The setup computations are assumed to be executed in exact arithmetic. (Concrete implementation details are described in [Section 6](#).)

6. Numerical results. Using the ideas described above, [Subsection 6.1](#) presents numerical results for two model problems that suggest that the precision bounds in [\(5.1\)](#) also apply in BFP-arithmetic. [Subsection 6.2](#) covers the a priori estimation of the individual BFP precisions $\tilde{w}_j, w_j, \dot{w}_j$, and compares multigrid convergence rates of fixed-precision floating point, fixed-precision BFP, and progressive-precision BFP setups. We also report on the estimation of γ and w_{tmp} to avoid recomputations in [Algorithm 1](#) ([Subsection 6.3](#)), and study the effect of skipping BFP-vector normalization altogether ([Subsection 6.4](#)).

With $\Omega := (0, 1)$ and $f \in L^2(\Omega^d)$, we consider the following model problems: find $u \in C^{2m}$ s.t.

$$(6.1) \quad \begin{aligned} -\Delta u &= f & \text{in } \Omega^d, \\ u &= 0 & \text{on } \partial(\Omega^d), \end{aligned} \quad (6.2) \quad \begin{aligned} u'''' &= f & \text{in } \Omega, \\ u &= u' = 0 & \text{on } \partial\Omega, \end{aligned}$$

where $d \in \{1, 2\}$, $m = 1$ in [\(6.1\)](#), and $d = 1$, $m = 2$ in [\(6.2\)](#). The biharmonic equation [\(6.2\)](#) is selected due to the rapidly growing condition number of the system matrix of the discrete problem, which is especially challenging for low-precision computations [\[19\]](#). Both model problems are approximated via the standard Rayleigh-Ritz finite element method, using identical, finite-dimensional trial and test spaces. For the discretization, we use B-spline finite elements of order $k = p + 1$, where p is the polynomial degree. The Dirichlet boundary conditions are enforced strongly. Overall, the setup follows [\[19\]](#). The manufactured solutions u are chosen as smooth functions with trigonometric components. All setup computations (including assembly of the linear system and [Algorithm 11](#)) are performed in high precision floating point arithmetic using a 400 bit mantissa to ensure sufficient accuracy. For comparison, double precision has a 53 bit mantissa and quad precision a 113 bit mantissa. Integrals are approximated via Gauss-Legendre quadrature, with $(p + 1)^d$ nodes and weights per element.

For all experiments, we use a prototype C++ BFP implementation based on the GNU Multiple Precision Arithmetic Library (GMP) offering arbitrarily wide integer types, and the GNU Multiple Precision Floating-Point Reliable Library (MPFR) for arbitrary precision floating point formats. Our implementation is experimental and favors flexibility over computational performance as the numerical results are the focus of this paper. Thus, we do not present any run time results.

6.1. Confirmation of BFP-precision bounds. It is desirable to estimate sufficient mantissa widths \tilde{w}_j, w_j , and \dot{w}_j before application of the solver. Given a specific problem, the asymptotic bounds in [\(5.1\)](#) and [\(5.2\)](#) are used for such a priori estimates. The objective of this section is the experimental confirmation of those bounds, to assert that they can in fact be used for a priori estimates in practice. To that end, the mantissa widths \tilde{w}_j, w_j , and \dot{w}_j are initially not estimated, but iteratively increased in steps of one bit per run of $\mathcal{IR}\mathcal{V}$ (starting from 1 bit) until the BFP-approximation is close to a reference solution for each level j . We compare the computed (BFP-) solution \tilde{u}_h to a reference u_h that is computed in floating point arithmetic using a 400 bit mantissa. We accept \tilde{u}_h if $\|u - \tilde{u}_h\|_{\mathcal{L}} / \|u - u_h\|_{\mathcal{L}} \leq 1.5$, where $\|\cdot\|_{\mathcal{L}} = a(\cdot, \cdot)^{1/2}$ is the energy norm and a is the bilinear form associated with the weak formulation. We aim for discretization accuracy, i.e., a total error of order $\mathcal{O}(h^{k-m})$. This is achieved

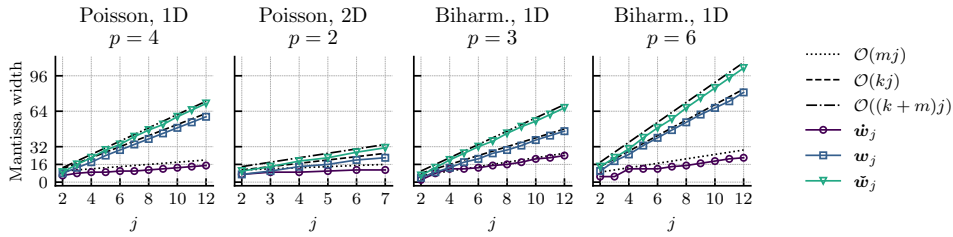


FIG. 3. Minimum number of bits required for the BFP mantissa to maintain optimal error convergence in the energy norm over grid refinement for four test cases using $\mathcal{IR}\text{-}\mathcal{V}$. The x-axis shows the refinement level with mesh sizes $h = 2^{-j}$.

for the reference solution. The prolonged exact solution of the next coarser grid is used as an initial guess, mimicking \mathcal{FMG} , and the number of \mathcal{IR} -iterations is limited to 50. This is an overly pessimistic limit for \mathcal{FMG} and, in most cases, a few iterations are sufficient.

In this initial experiment, we are interested in finding the smallest mantissa required to observe convergence and not in the convergence rate of the multigrid solver. Precisions that are sufficient to achieve discretization-error-accuracy do not necessarily lead to satisfactory convergence rates of the linear solver. Increasing the precision beyond what is required to achieve discretization-error-accuracy may further increase the convergence rates. Clearly, this rate is limited, and higher precision generally entails lower computational performance. In practice, a trade-off has to be made, which we revisit in [Subsection 6.2](#).

For simplicity in this section, we do not employ progressive precision inside the V-cycle itself, but apply the precision of the finest grid throughout the hierarchy for each run. First, we choose $w_j = \dot{w}_j = 200$ and determine the minimal width \check{w}_j over mesh refinement such that \check{u}_h fulfills the convergence criterion. Using the obtained precisions \check{w}_j , we fix $\dot{w}_j = 200$ and find the minimal w_j in the same way. Eventually using both \check{w}_j and w_j , we apply the same process to find the minimal \dot{w}_j . The results for four test cases are plotted in [Figure 3](#).

We observe that the asymptotic behavior in [\(5.2\)](#) that is predicted for floating point arithmetic in [\[13, 19\]](#) also holds for the BFP implementation. Note that the finite element polynomial order k is $p + 1$, where p is the polynomial degree. For the biharmonic equation with $p = 3$, we have $m = 2$, $k = 4$, and therefore expect (and observe) $\check{w}_j \in \mathcal{O}(6j)$, $w_j \in \mathcal{O}(4j)$, and $\dot{w}_j \in \mathcal{O}(2j)$. We do not see any asymptotic difference between the 1D and 2D cases (nor do we expect any), but we include the 2D Poisson test case to illustrate this.

6.2. A priori estimation of required BFP-precision. Selecting the precisions via the approach in [Subsection 6.1](#) is expensive and impractical for real applications. It is feasible, however, to estimate the precisions based on discretization-dependent constants that can be computed relatively cheaply on very coarse grids. Those estimated precisions are then extrapolated for finer grids according to their asymptotic behavior given in [\(5.1\)](#) and [\(5.2\)](#).

In this paper, we choose the precisions as follows. For w_j , we employ the estimation algorithm from [\[19\]](#). This algorithm could also be used with small adjustments to determine \dot{w}_j and \check{w}_j , but instead we propose to select \dot{w}_j and \check{w}_j subject to a certain target convergence rate of the solver. For that, we employ [Algorithm 2](#) with $j_c = 5$, $q_{\max} = 64$, and $\rho_{\text{thresh}} = 1.05$. The minima are determined using binary search over

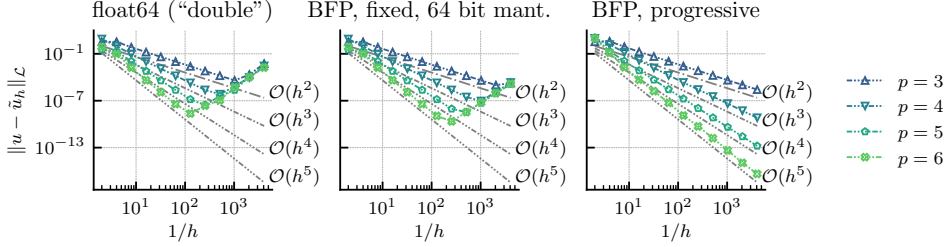


FIG. 4. Total error over refinement applying \mathcal{FMG} to the biharmonic model problem using different setups. The left plot shows the error evolution using standard 64 bit floating point precision; the plot in the center shows the results for BFP- \mathcal{FMG} , with fixed precision, i.e., $\tilde{w}_j = w_j = \dot{w}_j = 64$ for all levels $j = 1, \dots, 12$. Both fixed precision approaches lead to approximations that are eventually dominated by rounding errors. The plot on the right employs the progressive precision BFP- \mathcal{FMG} algorithm with estimated precisions. The corresponding computed solutions are discretization-error-accurate, regardless of the refinement level. As shown in [19], the same qualitative results are also achieved for progressive precision floating point implementations.

$\{1, \dots, q_{\max}\}$. On coarse levels j_c , this approach is reasonably fast.

Algorithm 2 BFP precision estimation: `bfp-prec-est`

Input: $j_c : \mathbb{Z}_{>0}$ (estimation level), $q_{\max} : \mathbb{Z}_{>0}$ (sufficient mantissa width for convergence),
 $\rho_{v,\text{thresh}} : \mathbb{R}$ (threshold for relative convergence rate), $m : \mathbb{Z}_{>0}$ ($2m =$ order of the PDE),
 $k : \mathbb{Z}_{>0}$ (approximation order), $w_j : \mathbb{Z}_{>0}$, $j = 1, \dots, \ell$ (precisions estimated as in [19])

- 1: $\tilde{w}_j(q) := j(m + k) + q$ ▷ Shorthand for (5.2) plus constant.
- 2: $\dot{w}_j(q) := jm + q$ ▷ Shorthand for (5.2) plus constant.
- 3: $\rho_{v,\text{ref}} \leftarrow \text{conv-rate-v-cycle}(\tilde{w}_j(q_{\max}), w_j, \dot{w}_j(q_{\max}), j_c)$
▷ Reference convergence rate on level j_c .
- 4: $\tilde{q} \leftarrow \min \{q \in \{1, \dots, q_{\max}\} : \text{conv-rate-v-cycle}(\tilde{w}_j(q), w_j, \dot{w}_j(q_{\max}), j_c) / \rho_{v,\text{ref}} < \rho_{v,\text{thresh}}\}$
▷ Min. additive constant for \tilde{w}_j to satisfy conv. crit.
- 5: $\dot{q} \leftarrow \min \{q \in \{1, \dots, q_{\max}\} : \text{conv-rate-v-cycle}(\tilde{w}_j(\tilde{q}), w_j, \dot{w}_j(q), j_c) / \rho_{v,\text{ref}} < \rho_{v,\text{thresh}}\}$
▷ Min. additive constant for \dot{w}_j to satisfy conv. crit.
- 6: **return** $(\tilde{w}_j(\tilde{q}), \dot{w}_j(\dot{q}))$

The convergence rate $\rho_v = \|V\|_A$ is computed as the square root of the largest generalized eigenvalue of $V^T A V x = \lambda A x$, where V is the error propagation matrix of \mathcal{V} . This matrix is constructed by applying \mathcal{V} to the canonical basis vectors. This is the same approach as taken in [19]. In Algorithm 2, `conv-rate-v-cycle`($\tilde{w}_j, w_j, \dot{w}_j, j$) computes ρ_v on level j , using progressive precision to construct V in BFP arithmetic.

In Figure 4, the progressive precision BFP- \mathcal{FMG} solver (right plot) is applied to the biharmonic equation and compared to a reference implementation using standard “double” precision 64 bit IEEE-754 floating point arithmetic (left plot), and a BFP- \mathcal{FMG} solver with fixed precision (center plot) on all levels. The results demonstrate the necessity of progressive precision, for both standard floating point and BFP implementations. For both fixed-precision \mathcal{FMG} solvers, we applied $N = 20$ \mathcal{IR} - \mathcal{V} iterations per level, which should be more than sufficient given the much smaller number of iterations that we need to achieve discretization-error-accuracy with the progressive precision BFP implementation. (The number of iterations for progressive precision BFP- \mathcal{FMG} is listed in Figure 5.) Note that the fixed precision BFP setup even performs slightly better than the floating point version for this test case. This can be explained by the different usage of the 64 bits: the 64 bit floating point format reserves only 53 bits for the mantissa, while the BFP format uses all 64 bits for the mantissa.

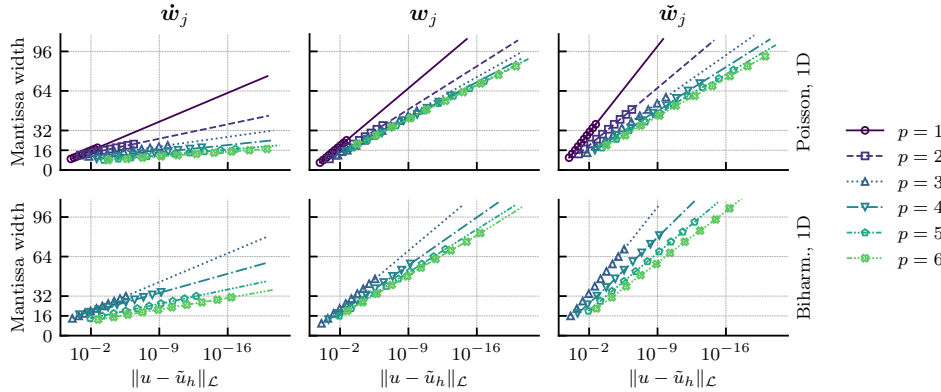


FIG. 5. *Progressive precision BFP-FMG using a priori estimated mantissa widths. The plots show the applied precisions to achieve a certain target accuracy. Markers indicate actual data points. All lines have been extrapolated. The number of $\mathcal{IR}\text{-}\mathcal{V}$ -iterations, N , per \mathcal{FMG} -level has been estimated according to [19] as $N = \{2, 1, 1, 3, 7, 15\}$ for the Poisson problem with $p = \{1, \dots, 6\}$ and as $N = \{2, 1, 2, 4\}$ for the biharmonic equation with $p = \{3, \dots, 6\}$. The estimates for N match the estimates that we obtained from a reference implementation that employs extremely accurate floating point arithmetic with mantissas using 400 bits. (IEEE-754 “double” precision uses 53 bit mantissas.) The number of iterations for higher polynomial degrees are larger than necessary in practice. For each data point in x -direction, a refinement step has been performed. The rightmost data points for each line correspond to a mesh size of $h \approx 2.5e-4$.*

Figure 5 shows the mantissa widths used to achieve a certain target accuracy in the energy norm when using progressive precision BFP-FMG. Asymptotically optimal grid convergence is observed under refinement for all cases. For the biharmonic equation, this is depicted in the right plot in Figure 4, which uses the same data. A comparison to the results of [19, Figures 2, 9] shows that the number of bits required to attain a certain target accuracy is similar to that of floating point arithmetic.

6.3. Choice of γ and w_{tmp} . Algorithm 1 (qcomp) requires the estimation of an upper bound γ of the infinity norm $\|z\|_\infty$ for the result z of (4.1), and the estimation of a sufficiently large mantissa width, w_{tmp} , for the temporary result. The objective is to choose these values as tight as possible, while still avoiding underflow and overflow along with the ensuing recomputation (see Algorithm 1, line 18).

In the following we discuss heuristics for choosing γ and w_{tmp} for the individual steps of Algorithms 12 to 14, with a focus on estimates for BFP-FMG. However, since $w_{\text{tmp}} \geq w_{\text{out}}$ we provide $w_{\text{add}}^* = w_{\text{tmp}} - w_{\text{out}}$ where w_{out} is level dependent while w_{add}^* is fixed across all levels.

To derive the heuristics, we make several simplifying assumptions that characterize an important class of problems, but hopefully carry over to more general cases. In particular, assume in the following that $\text{diag}(A) = I$ and that the entries of $E := I - A$ and the row sums of A are nonnegative. Note then that $\|E\|_\infty \leq 1$ and $\rho(A) \leq 2$. The $\mathcal{IR}\text{-}\mathcal{V}$ -iteration on one level of \mathcal{FMG} is indicated with superscript (i) , $i \in \{1, \dots, N\}$, if necessary. Applying $\mathcal{IR}\text{-}\mathcal{V}$ directly (without \mathcal{FMG}) may involve slightly different assumptions, but the overall approach is similar (see Subsection 6.4 and Remark 3).

The values of γ are based on various bounds and inequalities, while the values of w_{add}^* are determined empirically. In particular, w_{add}^* is chosen such that no recomputation is triggered during BFP-FMG on the finest level $j = 12$ for both 1D model problems and $p \in \{1, \dots, 6\}$ using the setup discussed in Subsection 6.2. The same value of w_{add}^* is then later used for all levels. The choices for γ and w_{add}^* are

summarized in [Table 1](#).

IR, residual (Algorithm 12, line 2). For a convergent *IR* process we generally expect the residual to steadily get smaller over time, but there is no guarantee that this will happen monotonically (which can lead to overflow), and occasionally large reductions may occur (which can lead to underflow). One could try to account for all of this, but we have found it to be best simply to choose w_{tmp} a little larger than w_{out} and assume that the residual does not increase. To be more specific, for iteration i , we choose

$$(6.3) \quad \gamma = \begin{cases} \|r_{\ell-1}^{(N)}\|_{\infty}, & i = 1, \\ \|r_{\ell}^{(i-1)}\|_{\infty}, & i > 1, \end{cases} \quad w_{\text{add}}^* = \begin{cases} 5, & i = 1, \\ 4, & i > 1, \end{cases}$$

where $r_{\ell-1}^{(N)}$ is the residual after *IR-V* iteration N on the next coarser *FMG*-level.

IR, correction (Algorithm 12, line 7). The bound for γ in this step follows from the triangle inequality. We choose $\gamma = \|x\|_{\infty} + \|y\|_{\infty}$, which works extremely well in practice, so that no bits have to be added, i.e., $w_{\text{add}}^* = 0$.

V, relaxation (Algorithm 13, line 2). Second-order Chebyshev relaxation has the form

$$(6.4) \quad y \leftarrow (c_1 I + c_2 A)r,$$

where c_1 and c_2 are scalar constants. Noting in [Algorithm 10](#) that $\alpha > 0, c > 0$, and

$$\beta = \left(1 + \frac{c}{\sqrt{2}\alpha}\right)\left(\alpha - \frac{c}{\sqrt{2}}\right) > \alpha - \frac{c}{\sqrt{2}} > \alpha - c = \eta\rho > 0$$

it follows that $c_1 > 0$ and $c_2 < 0$. Since $0 \leq A \leq 2I$, then $(c_1 + 2c_2)I \leq c_1 I + c_2 A < c_1 I$, which in turn implies that

$$(6.5) \quad \|y\|_{\infty}/\|r\|_{\infty} \in [c_1 + 2c_2, c_1].$$

We thus set $\gamma = c_1 \|r\|_{\infty}$. Using the lower bound for $\|y\|_{\infty}/\|r\|_{\infty}$, w_{tmp} could be chosen as

$$(6.6) \quad w_{\text{tmp}} = w_{\text{out}} + \left\lceil \log_2 \left(\frac{c_1}{c_1 + 2c_2} \right) \right\rceil.$$

In practice, simply adding $w_{\text{add}}^* = 2$ bits works well in our experience.

V, residual (Algorithm 13, line 4). Rewriting (6.4) as

$$y \leftarrow c_2 A r + c_1 r = c_2 (A - I)r + (c_1 - c_2)r = -c_2 E r + (c_1 - c_2)r$$

leads to the following bound on the subsequent relative residual norm:

$$(6.7) \quad \begin{aligned} \|Ay - r\|_{\infty}/\|r\|_{\infty} &\leftarrow \| -c_2 A E r + (c_1 - c_2) A r - r \|_{\infty}/\|r\|_{\infty} \\ &\leq \| -c_2 A E + (c_1 - c_2) A - I \|_{\infty} \\ &\leq 2c_2 + 2|c_1 - c_2| + 1 \\ &= 2c_1 + 1, \end{aligned}$$

where the last line follows because $c_1 > c_2$. This gives a liberal upper bound for the range, that is, a conservative estimate for γ . We therefore scale the bound empirically by $1/4$, and choose $\gamma = (1/4)(2c_1 + 1)\|r\|_{\infty}$. Unfortunately, there is no useful lower

TABLE 1

Concrete estimates employed for γ , and experimentally determined values for w_{add}^* for *Algorithm 1* (qcomp) in BFP-FMG. The number of additional bits $w_{\text{add}}^* = w_{\text{tmp}} - w_{\text{out}}$ is chosen minimally such that no recomputation is triggered on the finest level $j = 12$ for both 1D model problems and $p \in \{1, \dots, 6\}$. The individual heuristics are discussed in *Subsection 6.3*. N and $i \in \{1, \dots, N\}$ are used to indicate the number of \mathcal{IR} -iterations and the current \mathcal{IR} -iteration, if necessary.

Step	γ	w_{add}^*
\mathcal{IR} , residual (line 2)	$\begin{cases} \ r_{\ell-1}^{(N)}\ _{\infty}, & i = 1 \\ \ r_{\ell}^{(i-1)}\ _{\infty}, & i > 1 \end{cases}$	$\begin{cases} 5, & i = 1 \\ 4, & i > 1 \end{cases}$
\mathcal{IR} , correction (line 7)	$\ x\ _{\infty} + \ y\ _{\infty}$	0
\mathcal{V} , relaxation (line 2)	$c_1 \ r\ _{\infty}$	2
\mathcal{V} , residual (line 4)	$\frac{1}{4}(2c_1 + 1)\ r\ _{\infty}$	4
\mathcal{V} , restriction (line 5)	$\ R\ _{\infty} \ r_v\ _{\infty}$	6
\mathcal{V} , correction (line 8)	$\ y\ _{\infty} + \ d_{\ell-1}\ _{\infty}$	1
FMG, prolongation (line 6)	$\ x\ _{\infty}$	0

bound for $\|Ay - r\|_{\infty}/\|r\|_{\infty}$ because we cannot rule out the possibility that the error $e = y - A^{-1}r$ is very smooth (e.g., the minimal eigenvector), meaning that $\|Ay - r\|_{\infty}/\|r\|_{\infty}$ would be $\mathcal{O}(h^2)$. There seems to be little choice here but to use an initial $w_{\text{tmp}} \gg w_{\text{out}}$ and adjust it to a more conservative value based on the observed y as the cycles proceed. In practice, adding a few bits to w_{tmp} compared to w_{out} , however, works well. The hope is that the size of the residual after relaxation is somewhat consistent from one cycle to the next. We find $w_{\text{add}}^* = 4$ to be sufficient.

\mathcal{V} , restriction (*Algorithm 13, line 5*). The upper bound for the residual transfer follows from the triangle inequality, i.e., $\gamma = \|R\|_{\infty} \|r_v\|_{\infty}$. Here too we lack a useful lower bound on the range. Indeed, $Rr_v = 0$ is certainly possible. However, such a loss indicates that coarsening is really useless itself. Fortunately it is also unnecessary because the residual must be oscillatory and relaxation alone would have reduced it significantly. That is, it is probably sufficient to choose w_{tmp} only a little larger than w_{out} because little damage would be done by any loss of bits resulting from an inaccurate estimate. However, to avoid underflow in all cases, we find that we need to add $w_{\text{add}}^* = 6$ bits.

\mathcal{V} , interpolation and correction (*Algorithm 13, line 8*). For standard nodal-based interpolation, we can expect $\|Pd_{\ell-1}\|_{\infty} = \|d_{\ell-1}\|_{\infty}$, which gives γ (and w_{tmp}) exactly. Other forms of interpolation are probably at least approximately the same. For the correction, $y \leftarrow y - d$, an obvious upper bound on the range is again given by the triangle inequality. The range is less clear except for the initial correction when $y = 0$ so that the updated y has norm $\|y\|_{\infty} = \|d\|_{\infty}$. For later cycles, especially near convergence, a major reduction in the size of y would not be expected. This heuristic turns out to apply, and we set $\gamma = \|y\|_{\infty} + \|d_{\ell-1}\|_{\infty}$, only adding $w_{\text{add}}^* = 1$ bit.

FMG, interpolation (*Algorithm 14, line 3*). Same argument as for interpolation in \mathcal{V} . We set $\gamma = \|x\|_{\infty}$ and require no additional bits ($w_{\text{add}}^* = 0$).

One observation is that the heuristics for γ perform quite well. Although only a few (≤ 6) bits are added for the temporary vector, recomputations can be avoided altogether. The correction in \mathcal{IR} and the FMG prolongation remarkably do not require additional bits to prevent underflow. Also, for the \mathcal{V} -cycle correction and the relaxation, only a respective 1 and 2 additional bits are sufficient. The results of the residual computation in \mathcal{IR} and inside the \mathcal{V} -cycle, as well as the restriction, are less

TABLE 2

Number of calls to `qcomp` (Algorithm 1) that triggered recomputation during BFP-FMG on the finest level $j = 12$, using $w_{\text{tmp}} = w_{\text{out}} + \min(w_{\text{add}}^*, w_{\text{add}}^{\text{max}})$. The values of w_{add}^* are listed in Table 1 and are chosen minimally such that no recomputation is necessary. The total number of calls to `qcomp` on each level $j > 1$ is shown in parentheses.

PDE	$w_{\text{add}}^{\text{max}}$	$p = 1$	$p = 2$	$p = 3$	$p = 4$	$p = 5$	$p = 6$
Poisson 1D	∞	0 (13)	0 (7)	0 (7)	0 (19)	0 (43)	0 (91)
	4	0 (13)	0 (7)	0 (7)	0 (19)	0 (43)	0 (91)
	2	2 (13)	2 (7)	2 (7)	3 (19)	1 (43)	4 (91)
	0	9 (13)	3 (7)	4 (7)	11 (19)	24 (43)	47 (91)
Biharm. 1D	∞	-	-	0 (13)	0 (7)	0 (13)	0 (25)
	4	-	-	0 (13)	1 (7)	0 (13)	2 (25)
	2	-	-	4 (13)	1 (7)	4 (13)	5 (25)
	0	-	-	8 (13)	3 (7)	8 (13)	13 (25)

predictable. However, even for those computations, adding 4 bits still yields good overall results.

The bottom line is that, given some relatively simple estimates for the upper bounds, by adding only a few bits compared to w_{out} , recomputations can largely be avoided in BFP-FMG. Furthermore, the exact choice of how many bits to add is not critical. To illustrate this, Table 2 shows the number of recomputations triggered for other, smaller choices of w_{add}^* . Concretely, we show results for setting $w_{\text{tmp}} = w_{\text{out}} + \min(w_{\text{add}}^*, w_{\text{add}}^{\text{max}})$ for $w_{\text{add}}^{\text{max}} \in \{0, 2, 4\}$. In practice, simply choosing $w_{\text{add}}^* = 2$ for all operations yields a fairly small number of recomputations.

6.4. Skipping BFP-vector normalization. Algorithm 1 ensures that the results of BFP vector-vector and matrix-vector operations are exact up to the specified precision via normalization of the computed BFP-vector. The results above indicate that with proper estimates for γ and w_{tmp} , it provides a framework to build efficient discretization-error-accurate multigrid solvers in BFP arithmetic. Table 2 suggests that the estimates are, in fact, relatively accurate, and thus lead to the question whether normalization is necessary in the first place. To explore this, we elaborate on the accuracy of γ .

In the best case, that is, when the upper bound γ to the infinity norm of the result vector is estimated correctly ($\gamma = \|z\|_{\infty}$), the second part of Algorithm 1, after line 13, has no effect on the output. Consequently, just setting $w_{\text{out}} = w_{\text{tmp}}$ and returning after the first loop would yield the same result, but it avoids the second pass over the vector. So the global maximum MSB index μ^* is not required, and the atomic update in line 10 can be skipped as well. Depending on the block size, which for our studies is chosen maximally, avoiding the atomic update may have significant (positive) impact on (parallel) performance.

If the estimate for γ is a little too large, and we return early, some precision is lost, i.e., the result is computed accurately only to less than w_{out} bits. Table 2 shows that this just truncates the rightmost $w_{\text{tmp}} - w_{\text{out}}$ bits, i.e., 6 bits in extreme cases, but mostly much less than that. The hope is that this precision loss is insignificant and that it still leads to a discretization-error-accurate method, possibly at the cost of a slightly worse solver convergence rate.

If the estimate for γ is too small, we encounter overflow. The two's complement mantissa then wraps around, producing large errors in the result. This can be circumvented by saturation of the result to the range $[-2^{w_{\text{out}}-1}, 2^{w_{\text{out}}-1} - 1]$ of the two's

Algorithm 3 Non-normalized quantized BFP vector computation: `nnqcomp`**Input:** `setup-func`, `comp-func`, `input`, $w_{\text{out}} : \mathbb{Z}_{>0}$, $\gamma : \mathbb{B}^1$, $n : \mathbb{Z}_{>0}$ **Precondition:** $0 < w_{\text{out}}$, $\gamma > 0$, γ normalized**Local variables:** `setup`, $z^* : \mathbb{B}^1$ (exact result), $z_{\text{out}} : \mathbb{B}^n$ (result), μ_{out} , $\lambda_{\text{out}} : \mathbb{Z}$ \triangleright Allocation and setup.

- 1: $(z^*, \text{setup}) \leftarrow \text{setup-func}(\text{input})$ \triangleright Setup necessary variables for exact computations.
- 2: $\mu_{\text{out}} \leftarrow \text{msb}(\gamma_m) + \gamma_e - z_e^*$ \triangleright MSB of the estimated mantissa window.
- 3: $\lambda_{\text{out}} \leftarrow \mu_{\text{out}} - w_{\text{out}}$ \triangleright LSB of the estimated mantissa window.
- 4: $(z_{\text{out}})_w \leftarrow w_{\text{out}}$ \triangleright Width of result BFP vector.
- 5: $(z_{\text{out}})_e \leftarrow z_e^* + \lambda_{\text{out}}$ \triangleright Block-exponent of truncated result z_{out} .

 \triangleright Computation of the saturated and truncated result BFP vector.

- 6: **parallel for** $i = 1, \dots, n$ **do**
- 7: $z^* \leftarrow \text{comp-func}(z^*, \text{input}, \text{setup}, i)$ \triangleright Compute exact quantity in parallel.
- 8: $z_m^* \leftarrow z_m^* \gg \lambda_{\text{out}}$ \triangleright Shift and truncate exact result.
- 9: $z_m^* \leftarrow \text{clamp}(z_m^*, -2^{w_{\text{out}}-1}, 2^{w_{\text{out}}-1} - 1)$ \triangleright Saturate result.
- 10: $((z_{\text{out}})_m)_i \leftarrow \text{decr}(z_w^* - (z_{\text{out}})_w, z_m^*)$ \triangleright Cast result into output BFP vector.
- 11: **end parallel for**
- 12: **return** z_{out} \triangleright The result is saturated and truncated.

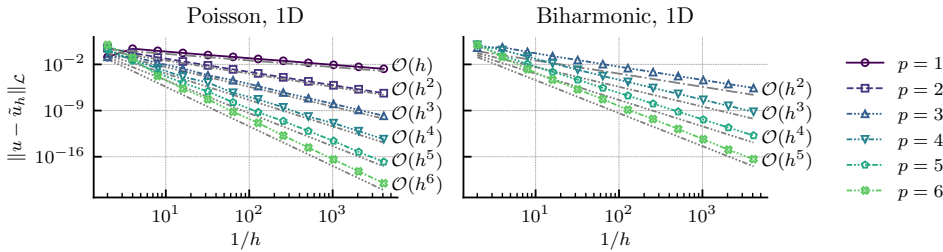


FIG. 6. Progressive precision BFP-FMG using the same setup as in Figure 5 but without BFP vector normalization, i.e., Algorithm 1 (`qcomp`) is replaced by Algorithm 3 (`nnqcomp`) for all vector operations on all refinement levels. Still, the solver produces discretization-error-accurate approximations in all tested cases. There is no significant error difference compared to the results computed with Algorithm 1.

complement integer. Then again, small deviations of γ from the actual infinity norm of the result are only leading to small errors in the computed vector.

These considerations are manifested in a modified version of Algorithm 1 (`qcomp`) listed in Algorithm 3 (`nnqcomp`). It skips the normalization step, and already returns after the first loop. The atomic update in Algorithm 1, line 10, is removed, the computed vector entries are saturated before being truncated to the target precision, and no temporary vector is required, saving the additional memory.

Figure 6 shows the total energy error over refinement using progressive precision BFP-FMG with Algorithm 3 instead of Algorithm 1. The heuristic estimates for γ are sufficient to ensure discretization-error-accuracy for both model problems, even without BFP-vector normalization. Direct comparison with the results using the safe Algorithm 1 shows no significant differences in error. We have briefly tested this also for higher order discretizations ($p = 10$), observing the same results.

REMARK 3 (Skipping normalization in $\mathcal{IR}\text{-}\mathcal{V}$). The situation is slightly different for $\mathcal{IR}\text{-}\mathcal{V}$ applied directly (i.e., without FMG) to a zero initial guess. During the first few (1-2) iterations, we observe that the infinity-norm of the \mathcal{IR} -residual (left-hand

side in [Algorithm 12](#), line 2) may in fact increase before it decreases. This increase may be so rapid that the estimates of γ from [Table 1](#) yield large overflows, leading to a diverging iteration. (This is especially pronounced for the lowest-order approximations, i.e., Poisson $p = 1$, and biharmonic $p = 3$; higher-order approximations are less problematic.) Using `qcomp` ([Algorithm 1](#)) instead of `nnqcomp` ([Algorithm 3](#)) only for the \mathcal{IR} -residual computation ([Algorithm 12](#), line 2) during the first few iterations of $\mathcal{IR}\text{-}\mathcal{V}$ fixes this issue, and we observe convergence for all test cases, if normalization is skipped for all remaining BFP-operations. Due to the initial approximation from the coarse grids, this is not necessary inside of \mathcal{FMG} .

Skipping BFP-vector normalization promises significant performance advantages in practice, without compromise regarding solution accuracy during \mathcal{FMG} . An iterative solver using [Algorithm 3](#) can additionally be equipped with a safety mechanism, that observes the residual convergence. Similar to the approach in [Remark 3](#), [Algorithm 1](#) can then be invoked dynamically, for certain operations, and for a subset of iterations, if the convergence stalls. However, as shown in [Figure 6](#), we do not observe that this is necessary for BFP- \mathcal{FMG} applied to our model problems.

7. Conclusion. This paper has demonstrated that the solution of elliptic PDEs in pure *integer arithmetic* can be done in practice. The results lay the groundwork for energy efficient implementations on specialized hardware. Additionally, the asymptotic precision bounds from [\[13, 19\]](#) have been applied successfully to obtain discretization-error-accuracy using a progressive- and mixed-precision multigrid solver in BFP format. To achieve this, we have proposed an efficient BFP-algorithm that ensures exact computation of common BLAS-like vector-vector and matrix-vector operations up to a specified precision. Compared to the results in [\[19, Figures 2, 9\]](#), the number of bits required to attain a certain level of error accuracy is similar to that of standard floating point arithmetic. BFP arithmetic is particularly efficient when applied to \mathcal{FMG} , since our results suggest that normalization of the BFP vectors is not necessary with proper estimates of upper bounds of the infinity norm of the intermediate results. Hopefully, all of this will stimulate future research in this area to establish a rigorous theoretical framework for iterative linear solvers in BFP arithmetic, and to develop accurate performance models with an eye towards deployment of these ideas for real applications.

REFERENCES

- [1] BASIC LINEAR ALGEBRA SUBPROGRAMS TECHNICAL FORUM, *Basic Linear Algebra Subprograms Technical Forum Standard*, International Journal of High Performance Applications and Supercomputing, 16 (2002), pp. 1–111, <https://journals.sagepub.com/toc/hpcc/16/1>.
- [2] A. BASUMALLIK, D. BUNANDAR, N. DRONEN, N. HARRIS, L. LEVKOVA, C. McCARTER, L. NAIR, D. WALTER, AND D. WIDEMANN, *Adaptive Block Floating-Point for Analog Deep Learning Hardware*, 2022, <https://doi.org/10.48550/arXiv.2205.06287>. Under submission at IEEE Transactions on Neural Networks and Learning Systems (TNNLS).
- [3] S. BOLDO, D. GALLOIS-WONG, AND T. HILAIRE, *A Correctly-Rounded Fixed-Point-Arithmetic Dot-Product Algorithm*, in Proceedings of the 27th IEEE Symposium on Computer Arithmetic, ARITH-2020, IEEE Computer Society, June 2020, pp. 9–16, <https://doi.org/10.1109/ARITH48897.2020.00011>.
- [4] S. DAI, R. VENKATESAN, H. REN, B. ZIMMER, W. J. DALLY, AND B. KHAILANY, *VS-Quant: Per-vector Scaled Quantization for Accurate Low-Precision Neural Network Inference*, in Proceedings of Machine Learning and Systems, A. Smola, A. Dimakis, and I. Stoica, eds., vol. 3 of MLSys, 2021, pp. 873–884, <https://proceedings.mlsys.org/paper/2021/file/f0935e4cd5920aa6c7c996a5ee53a70f-Paper.pdf>.
- [5] M. DRUMOND, T. LIN, M. JAGGI, AND B. FALSAFI, *Training DNNs with Hybrid Block Floating*

- Point*, in Proceedings of NeurIPS'18, S. Bengio, H. Wallach, H. Larochelle, K. Grauman, N. Cesa-Bianchi, and R. Garnett, eds., vol. 31 of Advances in Neural Information Processing Systems, Red Hook, NY, USA, 2018, Curran Associates Inc., p. 453–463, <https://proceedings.neurips.cc/paper/2018/file/6a9aeddfc689c1d0e3b9ccc3ab651bc5-Paper.pdf>.
- [6] GUSTAFSON AND YONEMOTO, *Beating Floating Point at Its Own Game: Posit Arithmetic*, Supercomputing Frontiers and Innovations: an International Journal, 4 (2017), p. 71–86, <https://doi.org/10.14529/jsfi170206>.
- [7] M. H. GUTKNECHT AND S. RÖLLIN, *The Chebyshev iteration revisited*, Parallel Computing, 28 (2002), pp. 263–283, [https://doi.org/10.1016/S0167-8191\(01\)00139-9](https://doi.org/10.1016/S0167-8191(01)00139-9).
- [8] M. HOROWITZ, *Computing's Energy Problem (and what we can do about it)*, in 2014 IEEE International Solid-State Circuits Conference Digest of Technical Papers (ISSCC), IEEE, Feb. 2014, pp. 10–14, <https://doi.org/10.1109/ISSCC.2014.6757323>.
- [9] N. P. JOUPPI, D. HYUN YOON, M. ASHCRAFT, M. GOTTSCHO, T. B. JABLIN, G. KURIAN, J. LAUDON, S. LI, P. MA, X. MA, T. NORRIE, N. PATIL, S. PRASAD, C. YOUNG, Z. ZHOU, AND D. PATTERSON, *Ten Lessons From Three Generations Shaped Google's TPUv4i : Industrial Product*, in 2021 ACM/IEEE 48th Annual International Symposium on Computer Architecture (ISCA), 2021, pp. 1–14, <https://doi.org/10.1109/ISCA52012.2021.00010>.
- [10] U. KÖSTER, T. J. WEBB, X. WANG, M. NASSAR, A. K. BANSAL, W. H. CONSTABLE, O. H. ELIBOL, S. GRAY, S. HALL, L. HORNOF, A. KHOSROWSHAHI, C. KLOSS, R. J. PAI, AND N. RAO, *Flexpoint: An Adaptive Numerical Format for Efficient Training of Deep Neural Networks*, in Proceedings of NIPS'17, I. Guyon, U. V. Luxburg, S. Bengio, H. Wallach, R. Fergus, S. Vishwanathan, and R. Garnett, eds., vol. 30 of Advances in Neural Information Processing Systems, Red Hook, NY, USA, 2017, Curran Associates Inc., p. 1742–1752, <https://proceedings.neurips.cc/paper/2017/file/a0160709701140704575d499c997b6ca-Paper.pdf>.
- [11] U. KULISCH, *Very fast and exact accumulation of products*, Computing, 91 (2011), pp. 397–405, <https://doi.org/10.1007/s00607-010-0131-y>.
- [12] X. LIAN, Z. LIU, Z. SONG, J. DAI, W. ZHOU, AND X. JI, *High-Performance FPGA-Based CNN Accelerator With Block-Floating-Point Arithmetic*, IEEE Transactions on Very Large Scale Integration (VLSI) Systems, 27 (2019), pp. 1874–1885, <https://doi.org/10.1109/TVLSI.2019.2913958>.
- [13] S. F. MCCORMICK, J. BENZAKEN, AND R. TAMSTORF, *Algebraic Error Analysis for Mixed-Precision Multigrid Solvers*, SIAM Journal on Scientific Computing, 43 (2021), pp. S392–S419, <https://doi.org/10.1137/20M1348571>.
- [14] S.-H. NOH, J. KOO, S. LEE, J. PARK, AND J. KUNG, *FlexBlock: A Flexible DNN Training Accelerator with Multi-Mode Block Floating Point Support*, 2022, <https://doi.org/10.48550/arXiv.2203.06673>. Under revision at IEEE Transactions on Computers.
- [15] S.-H. NOH, J. PARK, D. PARK, J. KOO, J. CHOI, AND J. KUNG, *LightNorm: Area and Energy-Efficient Batch Normalization Hardware for On-Device DNN Training*, 2022, <https://doi.org/10.48550/arXiv.2211.02686>.
- [16] B. PARHAMI, *Computer Arithmetic: Algorithms and Hardware Designs*, Oxford University Press, New York, 2nd ed., 2010.
- [17] S. QIAN ZHANG, B. MCDANEL, AND H. T. KUNG, *FAST: DNN Training Under Variable Precision Block Floating Point with Stochastic Rounding*, in 2022 IEEE International Symposium on High-Performance Computer Architecture (HPCA), IEEE, Apr. 2022, pp. 846–860, <https://doi.org/10.1109/HPCA53966.2022.00067>.
- [18] B. D. ROUHANI, D. LO, R. ZHAO, M. LIU, J. FOWERS, K. OVTCHAROV, A. VINOGRADSKY, S. MASSENGILL, L. YANG, R. BITTNER, A. FORIN, H. ZHU, T. NA, P. PATEL, S. CHE, L. CHAND KOPPAKA, X. SONG, S. SOM, K. DAS, S. TIWARY, S. REINHARDT, S. LANKA, E. CHUNG, AND D. BURGER, *Pushing the Limits of Narrow Precision Inferencing at Cloud Scale with Microsoft Floating Point*, in Proceedings of NeurIPS 2020, H. Larochelle, M. Ranzato, R. Hadsell, M. Balcan, and H. Lin, eds., vol. 33 of Advances in Neural Information Processing Systems, Curran Associates, Inc., November 2020, pp. 10271–10281, <https://proceedings.neurips.cc/paper/2020/hash/747e32ab0fea7fbd2ad9ec03daa3f840-Abstract.html>.
- [19] R. TAMSTORF, J. BENZAKEN, AND S. F. MCCORMICK, *Discretization-Error-Accurate Mixed-Precision Multigrid Solvers*, SIAM Journal on Scientific Computing, 43 (2021), pp. S420–S447, <https://doi.org/10.1137/20M1349230>.
- [20] J. H. WILKINSON, *Rounding Errors in Algebraic Processes*, Prentice-Hall series in Automatic Computation, Prentice-Hall, Englewood Cliffs, N. J., 1963.

Appendix A. Discrete Harmonic. Using the terminology in Section 3, suppose that v has minimum energy, $\|v\|_A$, subject to the constraint $\|v\|_\infty = 1$. To

estimate $\|v\|_A$, assume without loss of generality that v is 1 at grid point p : $v_p = 1$. Note that v is a discrete harmonic in the sense that $(Av)_q = 0$ for all grid points $q \neq p$. To see this, letting s be a scalar and $d \equiv (Av)_q$ for any $q \neq p$, we would then have that

$$\langle A(v - sd), v - sd \rangle = \langle Av, v \rangle - 2s\langle Av, d \rangle + s^2\langle Ad, d \rangle = \langle Av, v \rangle - 2s\|d\|^2 + s^2\langle Ad, d \rangle.$$

If d were not 0, then choosing $s > 0$ small enough (e.g., $s < \frac{\langle Ad, d \rangle}{\|d\|^2}$) would mean that $\langle A(v - sd), v - sd \rangle < \langle Av, v \rangle$, which contradicts optimality of v . Hence, $v = \gamma A^{-1}e_p$, where $\gamma = \frac{1}{\langle e_p, A^{-1}e_p \rangle}$ and e_p is the vector that is 1 at p and 0 elsewhere. (Note that v as defined here satisfies $v_p = \langle e_p, v \rangle = \gamma \langle e_p, A^{-1}e_p \rangle = 1$ and $v_q = \langle e_q, Av \rangle = \gamma \langle e_q, e_p \rangle = 0$ for $q \neq p$.) Thus,

$$\|v\|_A = \langle Av, v \rangle^{\frac{1}{2}} = \gamma \langle e_p, A^{-1}e_p \rangle^{\frac{1}{2}} = \gamma^{\frac{1}{2}} = \langle e_p, A^{-1}e_p \rangle^{-\frac{1}{2}}.$$

We therefore have that the minimum value of $\|v\|_A$ is the inverse square root of the maximum diagonal entry of A^{-1} .

Appendix B. BFP BLAS algorithms.

Algorithm 4 Exact axpby setup: eaxpby-setup

Input: $x : \mathbb{B}^n, y : \mathbb{B}^n, \alpha : \mathbb{B}^1, \beta : \mathbb{B}^1$

Local variables: $a^* : \mathbb{B}^1, b^* : \mathbb{B}^1, z^* : \mathbb{B}^1, d : \mathbb{Z}$

▷ Setup for the two products $a^* = \alpha x$ and $b^* = \beta y$.

- | | |
|--------------------------------------|------------------------------------|
| 1: $a_w^* \leftarrow \alpha_w + x_w$ | ▷ Widths of the products. |
| 2: $b_w^* \leftarrow \beta_w + y_w$ | |
| 3: $a_e^* \leftarrow \alpha_e + x_e$ | ▷ Block-exponents of the products. |
| 4: $b_e^* \leftarrow \beta_e + y_e$ | |

▷ Setup for the sum $z = a^* + b^*$.

- | | |
|--|---|
| 5: $d \leftarrow a_e^* - b_e^*$ | ▷ Difference of block exponents of αx and βy . |
| 6: if ($d < 0$) then | ▷ Aligning block-exponents of αx and βy . |
| 7: $z_w^* \leftarrow \max(a_w^*, b_w^* + d) + 1$ | |
| 8: else | |
| 9: $z_w^* \leftarrow \max(b_w^*, a_w^* + d) + 1$ | |
| 10: end if | |
| 11: $z_e^* \leftarrow \min(a_e^*, b_e^*)$ | ▷ Block-exponent of $z^* = \alpha x + \beta y$. |
| 12: return ($z^*, (a^*, b^*, d)$) | |
-

Algorithm 5 Exact axpby row: eaxpby-row

Input: $z^* : \mathbb{B}^1, (x : \mathbb{B}^n, y : \mathbb{B}^n, \alpha : \mathbb{B}^1, \beta : \mathbb{B}^1), (a^* : \mathbb{B}^1, b^* : \mathbb{B}^1, d : \mathbb{Z}), i : \mathbb{Z}_{>0}$

▷ Exact scalar multiplication.

- | | |
|--|--|
| 1: $a_m^* \leftarrow \alpha_m \cdot (x_m)_i$ | |
| 2: $b_m^* \leftarrow \beta_m \cdot (y_m)_i$ | |
| ▷ Exact addition. Requires alignment of block-exponents of a^* and b^* . | |
| 3: if ($d < 0$) then | ▷ $a_e^* < b_e^*$, resulting block-exponent is a_e^* . |
| 4: $b_m^* \leftarrow \text{incr}(d , b_m^*)$ | ▷ Ensure enough space to left-shift. |
| 5: $b_m^* \leftarrow b_m^* \ll d $ | ▷ Shifting mantissa to align exponents of a^* and b^* . |
| 6: else | ▷ $a_e^* \geq b_e^*$, resulting block-exponent is b_e^* . |
| 7: $a_m^* \leftarrow \text{incr}(d , a_m^*)$ | ▷ Ensure enough space to left-shift. |
| 8: $a_m^* \leftarrow a_m^* \ll d $ | ▷ Shifting mantissa to align exponents of a^* and b^* . |
| 9: end if | |
| 10: $z_m^* \leftarrow a_m^* + b_m^*$ | ▷ Computes exact sum $z_m^* = a_m^* + b_m^*$. |
| 11: return z^* | ▷ Return row i of the exact $\alpha x + \beta y$. |
-

Algorithm 6 Exact SpMV setup: `espmv-setup`

Input: $A : \mathbb{B}^{n \times m}$, $x : \mathbb{B}^m$, $m_A : \mathbb{Z}_{>0}$ (max. num. non-zeros per row of A)**Local variables:** $z^* : \mathbb{B}^1$ \triangleright Setup for the exact product Ax .

- 1: $z_w^* \leftarrow A_w + x_w + \lceil \log_2(m_A) \rceil$ \triangleright Width of mantissa of exact Ax .
 - 2: $z_e^* \leftarrow A_e + x_e$ \triangleright Block-exponent of exact Ax .
 - 3: **return** $(z^*, ())$
-

Algorithm 7 Exact SpMV row: `espmv-row`

Input: $z^* : \mathbb{B}^1$, $(A : \mathbb{B}^{n \times m}$, $x : \mathbb{B}^m$, $m_A : \mathbb{Z}_{>0}$), $(,)$, $i : \mathbb{Z}_{>0}$ **Local variables:** $t^* : \mathbb{X}_{A_w + x_w}$ \triangleright Exact dot product of one row of A and x .

- 1: $z_m^* \leftarrow 0$
 - 2: **for** $j \in \{[1, n] \cap \mathbb{Z}_{>0} : (\mathbf{A}_m)_{ij} \neq 0\}$ **do**
 - 3: $t^* \leftarrow (\mathbf{A}_m)_{ij} \cdot (\mathbf{x}_m)_j$ \triangleright Exact integer multiplications.
 - 4: $z_m^* \leftarrow z_m^* + t^*$ \triangleright Exact integer accumulation.
 - 5: **end for**
 - 6: **return** z^* \triangleright Return row i of the exact Ax .
-

Algorithm 8 Exact gemv setup: `egemv-setup`

Input: $A : \mathbb{B}^{n \times m}$, $x : \mathbb{B}^m$, $y : \mathbb{B}^n$, $\alpha : \mathbb{B}^1$, $\beta : \mathbb{B}^1$, $m_A : \mathbb{Z}_{>0}$ **Local variables:** $g^* : \mathbb{B}^1$, $z^* : \mathbb{B}^1$, \triangleright Reusing `espmv` and `eaxpby`.

- 1: $(g^*, \langle \text{empty} \rangle) \leftarrow \text{espmv-setup}(A, x, m_A)$ \triangleright Setup for $g^* = Ax$.
 - 2: $(z^*, (a^*, b^*, d)) \leftarrow \text{eaxpby-setup}(g^*, y, \alpha, \beta)$ \triangleright Setup for $\alpha g^* + \beta y$.
 - 3: **return** $(z^*, (g^*, a^*, b^*, d))$
-

Algorithm 9 Exact gemv row: `egemv-row`

Input: $z^* : \mathbb{B}^1$, $(A : \mathbb{B}^{n \times m}$, $x : \mathbb{B}^m$, $y : \mathbb{B}^n$, $\alpha : \mathbb{B}^1$, $\beta : \mathbb{B}^1$, $m_A : \mathbb{Z}_{>0}$),
 $(g^* : \mathbb{B}^1$, $a^* : \mathbb{B}^1$, $b^* : \mathbb{B}^1$, $d : \mathbb{Z}_{\geq 0}$), $i : \mathbb{Z}_{>0}$ \triangleright Reusing `espmv` and `eaxpby`.

- 1: $g^* \leftarrow \text{espmv-row}(g^*, (A, x, m_A), \langle \text{empty} \rangle, i)$ \triangleright Computing one row of Ax .
 - 2: $z^* \leftarrow \text{eaxpby-row}(z^*, (g^*, y, \alpha, \beta), (a^*, b^*, d), 1)$ \triangleright Computing one row of $\alpha Ax + \beta y$.
 - 3: **return** z^* \triangleright Return row i of the exact $\alpha Ax + \beta y$.
-

Appendix C. BFP multigrid algorithms.

Algorithm 10 Coefficients for two Chebyshev iterations

Input: ρ (upper bound for max. eigenvalue of generalized problem $Ax = \lambda Dx$), $0 < \eta < 1$ (part of spectrum to target)

- 1: $\alpha \leftarrow \frac{1}{2}(1 + \eta)\rho$
 - 2: $c \leftarrow \frac{1}{2}(1 - \eta)\rho$
 - 3: $\beta \leftarrow \alpha - \frac{c^2}{2\alpha}$
 - 4: $c_1 \leftarrow 2/\beta$
 - 5: $c_2 \leftarrow -1/(\alpha\beta)$
 - 6: **return** (c_1, c_2) \triangleright Return coefficients
-

Algorithm 11 Setup (\mathcal{S}) to ensure that $D = I$

Input: $A_i, b_i, 1 \leq i \leq \ell, P_j, 2 \leq j \leq \ell$ (prolongation operators), $\ell \geq 1$ (number of levels),
 ℓ_{est} (level on which the Chebyshev nodes are estimated),
 μ^* (part of the spectrum to target with the Chebyshev smoother)

- 1: $\rho \leftarrow \text{MaxGenEigenvalueUpperBound}(A_{\ell_{\text{est}}}, D_{\ell_{\text{est}}})$
- 2: $(c_1, c_2) \leftarrow \text{ChebyshevNodes}(\rho, \mu^*)$
- 3: $i \leftarrow \ell$ ▷ Initialize \mathcal{S}
- 4: $D_f \leftarrow \text{diag}(A_i)$
- 5: **while** $i > 0$ **do**
- 6: $A_i \leftarrow D_f^{-1} A_i$ ▷ Premultiply A by D so new $D = I$
- 7: $b_i \leftarrow D_f^{-1} b_i$ ▷ Preserve solution of fine-level equation
- 8: **if** $i > 1$ **then**
- 9: $D_c \leftarrow \text{diag}(A_{i-1})$
- 10: $R_i \leftarrow D_c^{-1} P_i^T D_f$ ▷ Preserve solution of correction equation
- 11: $D_f \leftarrow D_c$
- 12: **end if**
- 13: $i \leftarrow i - 1$ ▷ Decrement \mathcal{S} cycle counter
- 14: **end while**
- 15: **return** $(A_1, \dots, A_\ell, b_1, \dots, b_\ell, R_2, \dots, R_\ell, c_1, c_2)$

Algorithm 12 Iterative Refinement (\mathcal{IR}) with $D = I$

Input: A, b, x (initial guess), $\text{tol} > 0$ (convergence tolerance), $m_A, \text{InnerSolver}$

- 1: $(A, b) \leftarrow (\text{quant}(A), \text{quant}(b))$ ▷ Quantize to \tilde{w} bits
- 2: $r \leftarrow \text{qgemv}(A, x, b, 1, -1, m_A, \tilde{w})$ ▷ Compute \mathcal{IR} Residual $r \leftarrow Ax - b$
- 3: **if** $\|r\| < \text{tol}$ **then**
- 4: **return** x ▷ Return Solution of $Ax = b$
- 5: **end if**
- 6: $y \leftarrow \text{InnerSolver}(A, r)$ ▷ Approximate Solution y of $Ay = r$
- 7: $x \leftarrow \text{qsub}(x, y, w)$ ▷ Update Approximation $x \leftarrow x - y$
- 8: **goto** 2

Algorithm 13 $\mathcal{V}(1,0)$ -Cycle (\mathcal{V}) Correction Scheme with $D = I$

Input: $A, r, P, R, \ell \geq 1$ (number of \mathcal{V} levels); c_1, c_2 (Chebyshev coefficients), m_A, m_P, m_R

- 1: $(A, P, R) \leftarrow (\text{quant}(A), \text{quant}(P), \text{quant}(R))$ ▷ Quantize to \hat{w}_ℓ bits
- 2: $y \leftarrow \text{qgemv}(A, r, r, c_2, c_1, m_A, \hat{w}_\ell)$ ▷ Relax on Current Approximation ($y = 0$)
- 3: **if** $\ell > 1$ **then**
- 4: $r_v \leftarrow \text{qgemv}(A, y, r, 1, -1, m_A, \hat{w}_\ell)$ ▷ Evaluate \mathcal{V} Residual $r_v \leftarrow Ay - r$
- 5: $r_{\ell-1} \leftarrow \text{qspmv}(R, r_v, m_R, \hat{w}_\ell)$ ▷ Restrict \mathcal{V} Residual $r_{\ell-1} \leftarrow Rr_v$
- 6: $d_{\ell-1} \leftarrow \mathcal{V}(A_{\ell-1}, r_{\ell-1}, P_{\ell-1}, R_{\ell-1}, \ell - 1, m_A, m_P, m_R)$
- 7: ▷ Compute Correction from Coarser Levels
- 8: $y \leftarrow \text{qgemv}(P, d_{\ell-1}, y, -1, 1, m_P, \hat{w}_\ell)$ ▷ Interpolate & Update $y \leftarrow y - Pd_{\ell-1}$
- 9: **end if**
- 10: **return** y ▷ Return Approximate Solution of $Ay = r$

Algorithm 14 FMG(1,0)-Cycle (\mathcal{FMG}) with $D = I$

Input: $A, b, P, R, \ell \geq 1$ (number of \mathcal{FMG} levels),
 $N \geq 1$ (number of \mathcal{IR} cycles with one $\mathcal{V}(1,0)$ each), m_A, m_P, m_R

- 1: $x \leftarrow 0$ ▷ Initialize \mathcal{FMG}
- 2: **if** $\ell > 1$ **then** ▷ Check for Coarser Level
- 3: $x_{\ell-1} \leftarrow \mathcal{FMG}(A_{\ell-1}, b_{\ell-1}, P_{\ell-1}, R_{\ell-1}, \ell - 1, N, m_A, m_P, m_R)$
- 4: ▷ Compute Coarse-Level Approximation
- 5: $P \leftarrow \text{quant}(P)$ ▷ Quantize to w_ℓ bits
- 6: $x \leftarrow \text{qspmv}(P, x_{\ell-1}, m_P, w_\ell)$ ▷ Interpolate Approximation $x \leftarrow Px_{\ell-1}$
- 7: **end if**
- 8: $i \leftarrow 0$ ▷ Initialize \mathcal{IR}
- 9: **while** $i < N$ **do**
- 10: $x \leftarrow \mathcal{IR}(A, b, x, -1, m_A, \mathcal{V})$ ▷ Compute Correction by \mathcal{IR} - \mathcal{V}
- 11: $i \leftarrow i + 1$ ▷ Increment \mathcal{IR} - \mathcal{V} Cycle Counter
- 12: **end while**
- 13: **return** x ▷ Return Approximate Solution of $Ax = b$
